LAWRENCE
LIVERMORE
NATIONAL
LABORATORY

UCRL-JRNL-228439

# Effect of Pre-Equilibrium Spin Distribution on 48Ti Cross Sections

D. Dashdorj, T. Kawano, P. E. Garrett, J. A. Becker, U. Agvaanluvsan, L. A. Bernstein, M. B. Chadwick, M. Devlin, N. Fotiades, G. E. Mitchell, R. O. Nelson, W. Younes

February 28, 2007

Physical Review C

# Effect of Pre-Equilibrium Spin Distribution on $^{48}$Ti Cross Sections

D. Dashdorj,[1,2,†] T. Kawano,[3] P. E. Garrett,[2,4] J. A. Becker,[2] U. Agvaanluvsan,[2] L. A. Bernstein,[2] M. B. Chadwick,[3] M. Devlin,[3] N. Fotiades,[3] G. E. Mitchell,[1] R. O. Nelson,[3] and W. Younes[2]

[1]*North Carolina State University, Raleigh, NC 27695*
*Triangle Universities Nuclear Laboratory, Durham, NC 27708*
[2]*Lawrence Livermore National Laboratory, Livermore, CA 94551*
[3]*Los Alamos National Laboratory, Los Alamos, NM 87545*
[4]*Department of Physics, University of Guelph, Guelph, ON, N1G2W1 Canada*

(Dated: February 23, 2007)

## Abstract

Nuclear model calculations of discrete $\gamma$-ray production cross sections produced in $^{48}$Ti(n,n$'\gamma_i$)$^{48}$Ti and $^{48}$Ti(n,2n$\gamma_i$)$^{47}$Ti reactions were made as a function of incident neutron energy from $E_n = 1$ MeV to 35 MeV and compared with new experimental results using the large-scale Compton-suppressed Germanium Array for Neutron Induced Excitations (GEANIE) at LANSCE. The Hauser-Feshbach reaction code GNASH, incorporating the spin distribution for the pre-equilibrium process calculated with the Feshbach-Kerman-Koonin (FKK) quantum-mechanical pre-equilibrium theory, was used to calculate partial $\gamma$-ray transition cross sections. The comparisons of calculated and experimental data demonstrate that, the FKK model for pre-equilibrium leads a better overall reproduction of the experimental data above $E_n = 10$ MeV, where pre-equilibrium processes are important. The FKK calculation predicts a strong reduction in the high-spin state population in $^{48}$Ti by inelastic scattering. Population of low-spin states were also affected, however the change in the low-lying 983.5-keV ($2^+$) state production is small because almost all $\gamma$-ray decay cascades feed this transition. In addition, the FKK calculation has a significant impact on the partial $\gamma$-ray transition cross sections for the (n,2n) reaction above $E_n = 15$ MeV. The calculated cross sections for high-spin states in $^{47}$Ti are reduced, and those from the low-spin states are enhanced, in agreement with the experimental data.

PACS numbers: 24.10.-i 24.60.Gv 25.40.Fq 27.40.+z

[†]Electronic address: dashdorj1@llnl.gov

## I. INTRODUCTION

Analysis of cross sections measured at Los Alamos Neutron Science Center (LANSCE) with the GErmanium Array for Neutron Induced Excitations (GEANIE) [1] has demonstrated that the spin distribution of the residual nucleus following neutron-induced reactions has a significant influence on the $\gamma$-ray production probability [2, 3]. This is especially true when a high-spin state is involved, such as is often the case with isomers. A realistic treatment of the spin distribution should improve the accuracy of calculations of $\gamma$-ray production cross sections with the statistical Hauser-Feshbach model. Classical theories such as the exciton model [4, 5] are still widely used to predict the relative contributions of pre-equilibrium to the total reaction cross sections, because their model parameters are fitted to available experimental data. However, since classical approaches generally do not allow a natural treatment of spin transfer, we employ a quantum mechanical approach in this paper.

The pre-equilibrium process may be modeled using a multistep-direct reaction theory in which the bombarding projectile, that remains in the continuum, initiates a series of particle-hole ($ph$) excitations in the target nucleus. There are several well-known statistical multistep-direct (MSD) theories: Feshbach, Kerman, and Koonin [6] (FKK), Tamura, Udagawa, and Lenske [7] (TUL), and Nishioka, Weidenmüller, and Yoshida [8] (NWY). These theories employ different statistical assumptions for an intermediate state in the multistep reactions. The statistical assumptions employed in these various theories are still under debate, but differences between the theories occur mainly for reactions at high incident energies. Descriptions of the first step (one-step creating a $1p1h$ excitation) are very similar in principle [9]. At low energies ($E_{in} \leq 30$ MeV), the one-step direct process and the multistep compound (MSC) process, where the projectile is no longer in the continuum, can be employed to analyze experimental data.

The present data used for comparison with model calculations consist of partial $\gamma$-ray cross sections measured in the $n+^{48}$Ti reaction. The $\gamma$-ray transition cross sections produced by neutron-induced reactions on $^{48}$Ti were measured [10] at LANSCE with the GEANIE detector array. Since the level scheme of $^{48}$Ti is well known, and $^{48}$Ti does not have low-lying

isomeric states, comparison of experimental data with calculations provides a good test of the quantum mechanical theories for the pre-equilibrium process.

Excited states in residual $^{48}$Ti nuclei populated by neutron inelastic scattering can be formed through either a compound $^{49}$Ti$^*$ nucleus that decays by neutron evaporation, or a pre-equilibrium process that proceeds mainly through the creation of a $1p1h$ pair. These two processes produce rather different spin distributions; the momentum transfer via the pre-equilibrium process is smaller than in the compound reaction. This difference in the spin population should have a significant impact on the $\gamma$-ray de-excitation cascade, and therefore on the partial $\gamma$-ray cross sections. The spin distribution in the pre-equilibrium process is calculated with the FKK model, and the calculated spin distribution is combined with the GNASH Hauser-Feshbach statistical model calculations [11]. In order to examine the influence of the FKK calculation, the cross sections are also calculated assuming the entire spin distribution in the pre-equilibrium process to be the same as for the compound process. In the past such an assumption has often been made for Hauser-Feshbach plus exciton model calculations. Comparisons of $\gamma$-ray production cross sections for neutron induced reactions on $^{48}$Ti for incident neutron energies $E_n = 1$ MeV to 35 MeV are presented.

## II. CALCULATION METHOD

### A Spin distribution in the pre-equilibrium process

The $\gamma$-ray production cross sections are calculated with the GNASH code [11]. GNASH calculates the pre-equilibrium process with the exciton model, which is based on a classical theory and does not calculate spin transfer. However, it is known that the exciton model gives the fraction of pre-equilibrium to total particle emission reasonably well, and in fairly good agreement with energy-spectrum shapes calculated with FKK. We employ the exciton model for the energy-spectra calculations, and the spin distribution in the residual nucleus is replaced by the distribution calculated with the FKK theory.

The one-step MSD cross section is given by

$$\frac{d^2\sigma}{d\Omega dE} = \sum_J \frac{2J+1}{2s_a+1}\frac{\mu_a\mu_b}{(2\pi\hbar^2)^2}\frac{k_b}{k_a} \times \overline{\sum_{mm_bm_a} |T_J^{mm_bm_a}(\theta)|^2}\rho(1,1,E_x,J), \quad (1)$$

where $a$ and $b$ stand for incoming/out-going particles, $k$ is the wave number, $\mu$ the reduced mass, $m$ the $z$-component of spin, $T_J^{mm_bm_a}(\theta)$ the DWBA matrix elements $\langle\psi_f|f_\lambda(r)|\psi_i\rangle$ which excite a 1-particle 1-hole state ($1p1h$) where $f_\lambda(r)$ is the particle-hole excitation form factor, $J$ the total angular momentum transfer, and $\rho(1,1,E_x,J)$ the $1p1h$ state density in the residual system at the excitation energy $E_x$. The one-step calculation of Eq. (1) gives a spin-dependent population of continuum states in $^{48}$Ti. Since the ground-state spin of $^{48}$Ti is zero, the spin distribution in the continuum populated by the one-step MSD process is the same as the $J$-dependence of the MSD angle-integrated cross sections.

The MSD calculation employed here is similar to the modeling of Koning and Chadwick [12], and the present implementation is reported elsewhere [13]. The MSC component in the present analysis is assumed to have the same spin distribution as the compound process, since the MSC component has an angular distribution symmetric about 90° in the c.m. system, and the magnitude is usually smaller than MSD [14, 15].

The calculated one-step MSD FKK spin distributions are expressed by a Gaussian form

$$R_{\rm MSD}(J) = \frac{J+1/2}{\sigma^2}\exp\left\{-\frac{(J+1/2)^2}{2\sigma^2}\right\}, \quad (2)$$

where $\sigma^2$ is a spin cut-off parameter. An example is shown in Fig. 1, which shows a calculated spin distribution for $^{48}$Ti inelastic scattering at incident neutron energy 20 MeV, and out-going neutron energy of 11 MeV. The solid histogram is the FKK result, and the dotted histogram is the spin distribution resulting from the compound reaction. The FKK spin distribution is peaked at lower $J$-values – a high-spin state is difficult to make with a simple $1p$-$1h$ configuration in a single-particle model.

The Gaussian form of Eq. (2) is fitted to the FKK results with various neutron incident and out-going energies in order to obtain the spin cut-off parameter $\sigma^2$ as a function of excitation energy $E_x$. This is shown in Fig. 2.

## B FKK-GNASH calculation

The statistical Hauser-Feshbach model code, GNASH, is used to calculate the $\gamma$-ray production cross sections for neutron inelastic scattering on $^{48}$Ti. The particle transmission coefficients are calculated using the global optical potentials of Koning and Delaroche [16] for the neutrons and protons, and the $\alpha$-particle optical potential of Avrigeanu, Hodgson, and Avrigeanu [17]. The direct inelastic scattering cross sections are calculated for the $0^+$-$2^+$-$4^+$-$6^+$ rotational band members, assuming that the coupled-channels potential is similar to the spherical potential of Koning and Delaroche [16] with deformation parameters, $\beta_2 = 0.269$ and $\beta_4 = 0.150$. The deformation parameters are taken from the Reference Input Parameter Library version 2, RIPL-2 [18]. The direct cross sections to the 3.062 MeV ($2^+$) and 3.359 MeV ($3^-$) levels are calculated with the DWBA method. The $\gamma$-ray transmission coefficients are re-normalized to the $\gamma$-ray strength function $2\pi\langle\Gamma_\gamma\rangle/D_0$, where the $D_0$ value of 18.3 keV is adopted from [19] and $\langle\ \Gamma_\gamma\ \rangle = 1.4$ eV is taken from RIPL-2 [18].

The level scheme of $^{48}$Ti and the $\gamma$-ray branching ratios are taken from the Table of Isotopes [20] and RIPL-2 [18]. The discrete levels of $^{48}$Ti are included up to 5.1973 MeV ($8^+$). However, the $\gamma$-ray branching data are not complete above 4 MeV excitation energy. For some of the discrete levels above 2.5 MeV in $^{48}$Ti, the $\gamma$-ray branching ratios are unknown, and they are assumed to decay to the ground-state directly in RIPL-2. Thus causing a slight decrease in the calculated $2^+ \rightarrow 0^+$ transition cross section. In this case, a modest modification of the (unmeasured) $\gamma$-ray branching ratios has been done by considering some excited states that have the same spin and the measured $\gamma$-ray branching ratios. For example, the 4.102 MeV ($1^+$) state in RIPL-2 decays to the ground-state, but in the present calculations it was assumed to decay 50% to the ground-state and 50% to the first excited level, because the measured branching ratios of the 3.7385 MeV ($1^+$) state are 65% (ground-state) and 27% (first excited state).

The level density parameters, $a$, were the default values [11] except for $^{48}$Sc. The $a$ parameter for $^{48}$Sc in the GNASH code was slightly modified within the range of uncertainty (reduced by about 10%) in order to reproduce experimental $(n,p)$ cross sections near $E_n =$

14 MeV.

The spin distribution, $R(E_x, J)$, in the initial population is given by

$$R(E_x, J) = f_p(E_x) R_{\rm PE}(E_x, J) + (1 - f_p(E_x))\, R_{\rm CN}(E_x, J), \quad (3)$$

where $R_{\rm PE}$ and $R_{\rm CN}$ are the spin distributions for the pre-equilibrium and compound processes, respectively, and $f_p(E_x)$ is the fraction of pre-equilibrium to the total neutron emission. Because the assumption is made that MSC has the same spin distribution as CN,

$$R(E_x, J) = (f_p(E_x) - f_c(E_x))\, R_{\rm MSD}(E_x, J) + (1 - f_p(E_x) + f_c(E_x))\, R_{\rm CN}(E_x, J), \quad (4)$$

where $f_c(E_x)$ is the fraction of MSC, and $R_{\rm MSD}$ is given by the Gaussian form of Eq. (2). The fraction of pre-equilibrium cross section $f_p(E_x)$ is calculated with the exciton model, and the strength of the pre-equilibrium neutron emission is adjusted to the experimental neutron emission spectrum for $^{nat}$Ti [21], which helps determine the overall magnitude of pre-equilibrium emission in the reaction.

Figure 3 shows the calculated summed spin distributions in the $^{48}$Ti continuum that are excited by 20-MeV neutron inelastic scattering. In the past, nuclear model calculations unphysically assumed that the spin distributions in the pre-equilibrium process were the same as in the compound reaction. The spin distribution predicted for the compound nuclear reaction only is shown in the top panel of Fig 3. With the quantum mechanical theories of the pre-equilibrium process, the spin distribution can be calculated on a more realistic basis. The sum of the FKK pre-equilibrium and compound is shown in the bottom panel. As demonstrated here, the excited nucleus has a spin distribution that is peaked at lower $J$-values when the excitation energy is low.

## III. EXPERIMENTAL SETUP

The experimental data were obtained at the LANSCE Weapons Neutron Research (WNR) facility. Spallation neutrons are produced at the WNR facility by bombarding a natural tungsten target with the 800-MeV pulsed proton beam from the LANSCE linac. The pulse structure in this experiment consisted of micropulses 1.8-$\mu$s apart, bunched into macropulses

625-$\mu$s in duration. Spallation neutrons with energies ranging from a few keV to nearly 800 MeV are produced. The scattering sample consisted of 3.3 grams of $TiO_2$ enriched to 99.81% $^{48}$Ti in the form of a 2.4-cm diameter disk. The $\gamma$ rays were detected with the GEANIE (GErmanium Array for Neutron Induced Excitations) spectrometer, located 20.34 m from the neutron source on the 60° right flight path. For this experiment the GEANIE spectrometer consisted of 11 planar and 15 $\sim$ 20 - 25% High-purity Ge (HPGe) coaxial detectors. All of the planar detectors and 9 of the coaxial detectors were equipped with Compton suppression shields. A fission chamber with $^{235,238}$U foils [22] was located 2 m upstream from the GEANIE spectrometer and fission chamber events were used to determine the neutron flux.

Neutron energies were determined by the time-of-flight (TOF) technique. The data were collected for 6 days and a total of about $4.6\times10^8$ single- and higher-fold events were recorded. The excitation functions were obtained by applying TOF gates 15-ns wide on the $\gamma$-ray events in the interval to $E_n$ = 1 to 35 MeV. The $\gamma$-ray absolute efficiency curves for planar and coaxial detectors were calculated for GEANIE data using a Monte-Carlo simulation of the array [24]. As a validation of the experimental and analysis techniques, the partial cross sections of the $2_1^+ \rightarrow 0_1^+$ transition in $^{56}$Fe were extracted from a series of runs with the $^{48}$Ti sample sandwiched between 5-mil $^{nat}$Fe foils. These data were compared to the evaluated cross section of 705 $\pm$ 56 mb at $E_n$ = 14.5 MeV, determined by Nelson *et al.* [23]. The partial cross sections extracted for $2_1^+ \rightarrow 0_1^+$ transition from planar detectors ($\sigma_\gamma$(847-keV) = 761 $\pm$ 42 mb) and coax detectors ($\sigma_\gamma$(847-keV) = 742 $\pm$ 46 mb) data were consistent, within errors, with previous work [23]. More details about the experimental setup and the data analysis can be found in Ref. [3, 10].

## IV. RESULTS AND DISCUSSIONS

The partial level scheme of the $\gamma$-ray cascade in $^{48}$Ti is shown in Fig. 4. Comparisons of the partial $\gamma$-ray cross sections for the 983-keV ($2_1^+ \rightarrow 0_1^+$), 1312-keV ($4_1^+ \rightarrow 2_1^+$), 1037-keV ($6_1^+ \rightarrow 4_1^+$), and 1213-keV ($8_1^+ \rightarrow 6_1^+$) ground-state-band transitions in $^{48}$Ti are shown in

Figs. 5 – 8. Figure 5 displays the $2_1^+ \rightarrow 0_1^+$ transition. After neutron inelastic scattering, excited $^{48}$Ti$^*$ decays by emitting $\gamma$ rays, and almost ($\geq 95\%$) all decaying cascades proceed through this transition. The $2_1^+ \rightarrow 0_1^+$ $\gamma$-ray cross section is taken to represent the total inelastic cross section. The calculated $2_1^+ \rightarrow 0_1^+$ $\gamma$-ray cross section with and without the FKK spin distribution are almost identical up to 15 MeV and the difference remains small at higher neutron bombarding energies, as shown in Fig. 5. Since both calculations agree with experimental $2_1^+ \rightarrow 0_1^+$ data well, this provides evidence that the summed neutron emission cross sections are reasonably well calculated.

For higher-spin residual states (Figs. 6 – 8) the use of the FKK spin distribution has a large effect on the $\gamma$-ray production cross sections, reducing the calculated $\gamma$-ray production cross sections for higher spin states above $E_n = 10$ MeV. As shown in Fig. 3 (lower panel) the FKK calculation has lower angular momentum transfer to the nucleus, and the population of high-spin states in the continuum is suppressed. Therefore, the cross sections of $\gamma$-ray transitions from high-spin states are strongly suppressed. The effect is larger for the higher-excited $6^+$ states, an example of which ($6_2^+ \rightarrow 4_1^+$) is shown in Fig. 8. There is no effect at low incident energies ($E_n < 10$ MeV) because the reaction mechanism is dominated by the compound nucleus reaction. The FKK-GNASH calculation underestimates the experimental data above 20 MeV and near the peak cross section of the yrast $6_1^+ \rightarrow 4_1^+$ transitions as shown in Fig. 7. Changing the model parameters to reproduce the peak cross sections in Fig. 7 destroys the good agreement for the other partial cross sections. This indicates deficiencies remaining the modeling. These deficiencies have no straightforward solution. As shown in Figs. 6 – 8, all of the cross sections are reduced by including the FKK spin distribution. This reduction is compensated by an increase in the $\gamma$-ray production cross sections between two low-spin states, as the example of which is shown in Fig. 9 for the $1_1^+ \rightarrow 0_1^+$ transition.

With the FKK spin distribution, the same effect is also seen in the $\gamma$-ray production cross sections of $(n, 2n)$ reaction channel, namely the $\gamma$ transition cross sections for the high-spin residual states are reduced, and those for the low-spin transitions are increased. This effect is more clearly observed in the $(n, 2n)$ reaction than the $(n, n')$ reaction because pre-equilibrium emission becomes larger in the higher incident neutron energy region, where the

$(n, 2n)$ channel has opened up. Figure 10 shows the 159.4-keV $\gamma$-ray production cross section, which is the transition from the first excited state of $^{47}$Ti to the ground state. Although the spin of the first excited state, $7/2^-$ is not large, the FKK+GNASH calculation results in a lower cross section, in very good agreement with the experimental data. This reduction is due to the lower production cross sections of 1093.0- and 1284.9-keV cascade $\gamma$-rays that feed the 159.4-keV $7/2^-$ state, as an example in Fig. 11, originating from the $9/2^-$ state and the $11/2^-$ state, respectively. The production cross sections of these relatively high-spin states in $^{47}$Ti are suppressed because the fraction of high-$J$ states in $^{48}$Ti is reduced. Besides the reduction in high-spin state population, the FKK+GNASH calculation increases the low-spin state production. In Figs. 12 and 13, the $\gamma$-ray production cross sections for the 1549.8-keV $3/2^-$ to 159.4-keV $5/2^-$ and 1825.0-keV $(3/2)^+$ to ground state transitions are compared with the experimental data. The FKK+GNASH calculation gives about 60% larger cross section above 20 MeV consistent with the experimental data. As shown in Figs. 10 – 13, the experimental $\gamma$-ray production cross sections for low-lying states are well produced by including the FKK spin distribution in the pre-equilibrium process.

The spin distribution in the pre-equilibrium process also has an impact on the isomer production [2]. If the residual nucleus in the $(n, 2n)$ reaction has a high-spin isomer, the production cross section for this state would be reduced by including the FKK spin distribution. It is also possible to reduce the high-spin isomer production cross section without FKK calculations by just using a compound nucleus description and a spin cut-off parameter $\sigma^2$ in the level density formula which is unphysically reduced. The spin cut-off parameter is given by [25]

$$\sigma^2 = \frac{\mathcal{I}}{\hbar^2} T, \tag{5}$$

where $\mathcal{I}$ is the moment of inertia, and $T$ is the nuclear temperature. The moment of inertia is often expressed by $\mathcal{I} = \eta \mathcal{I}_{\rm rigid}$, where $\mathcal{I}_{\rm rigid}$ is the rigid-body moment of inertia. The $\eta$ value of $0.5 \sim 1.0$ is often used in the analysis of spin distributions of low-lying states [18, 26]. Al-Abyad *et al.* [27] showed that to reproduce the experimental isomeric ratio in the $^{196,198}$Hg(n,2n) reactions, it was necessary to use an $\eta$ value of 15–20%. This rather strong artificial modification to the $\sigma^2$ value results from the use of an improper pre-equilibrium

spin distribution, i.e. the compound nucleus.

## V. SUMMARY

In summary, the spin distribution of the states populated in the pre-equilibrium process in $^{48}$Ti + n reactions was calculated using the quantum mechanical theory of Fechbach-Kerman-Koonin (FKK). The FKK spin distribution was incorporated into Hauser-Feshbach statistical code GNASH and the $\gamma$-ray production cross sections were calculated and compared with experimental data. The difference in the partial $\gamma$-ray cross sections for spin distributions with and without pre-equilibrium effects is significant. The probability of $\gamma$-ray transitions from a high-spin state is strongly suppressed for the neutron incident energies $E_n > 10$ MeV because of the pre-equilibrium spin distribution. The effect is more clearly observed in the $(n, 2n)$ reaction channel than the $(n, n')$ reaction channel since the pre-equilibrium emission becomes larger for high neutron energy region, where the $(n, 2n)$ channel opens up. The calculated $\gamma$-ray transition probabilities from the high spin states in $^{47}$Ti are reduced, and those from the low-spin states are enhanced. While there are significant discrepancies remain for $\gamma$-rays from the $(n, n')$ channel, an impressive agreement is achieved for the $(n, 2n)$ channel.

## VI. ACKNOWLEDGMENTS

We would like to thank J. Wilhelmy for suggesting that the GEANIE data can provide useful insights into pre-equilibrium reaction mechanisms. This work was supported in part (for NCSU/TUNL) by the U.S. Department of Energy Grants No. DE-FG52-06NA26194 (NNSA Academic Alliance) and No. DE-FG02-97-ER41042, and the National Science and Engineering Research Council (Canada). Work performed, in part, under the auspices of the U.S. DoE by University of California, Lawrence Livermore National Laboratory under contract No. W-7405-ENG-48. Work performed, in part, under the auspices of the U.S. DoE by Los Alamos National Security, LLC, Los Alamos National Laboratory under Contract No. DE-AC52-06NA25396.

**REFERENCES**


[1] J. A. Becker, R. O. Nelson, Nucl. Phys. News Int. **7**, p.11 (1997).

[2] T. Kawano, P. Talou, M. B. Chadwick, Nucl. Instr. Methods A, **562**, 774 (2006).

[3] D. Dashdorj, Ph.D. thesis, North Carolina State University (2005).

[4] J. J. Griffin, Phys. Rev. Lett. **17**, 478 (1966).

[5] E. Gadioli, P. E. Hodgson "Pre-Equilibrium Nuclear Reactions," Clarendon Press, Oxford (1992).

[6] H. Feshbach, A. Kerman, S. Koonin, Ann. Phys. (N.Y.) **125**, 429 (1980).

[7] T. Tamura, T. Udagawa, H. Lenske, Phys. Rev. C **26**, 379 (1982).

[8] H. Nishioka, H. A. Weidenmüller, S. Yoshida, Ann. Phys. (N.Y.) **183**, 166 (1988).

[9] A. J. Koning, J. M. Akkermans, Ann. Phys. (N.Y.) **208**, 216 (1991).

[10] D. Dashdorj *et al.*, Nucl. Sci. Eng. *in press* (2007).

[11] P. G. Young, E. D. Arthur, M. B. Chadwick, LA-12343-MS, Los Alamos National Laboratory (1992).

[12] A. J. Koning, M. B. Chadwick, Phys. Rev. C **56**, 970 (1997).

[13] T. Kawano, T. Ohsawa, M. Baba, T. Nakagawa, Phys. Rev. C **63**, 034601 (2001).

[14] T. Kawano, Phys. Rev. C **59**, 865 (1999).

[15] M. B. Chadwick, P. G. Young, Phys. Rev. C **47**, 2255 (1993).

[16] A. Koning, J. P. Delaroche, Nucl. Phys. **A713**, 231 (2003).

[17] V. Avrigeanu, P. Hodgson, M. Avrigeanu, Phys. Rev. C **49**, 2136 (1994).

[18] Reference Input Parameter Library, RIPL-2, IAEA-TECDOC, International Atomic Energy Agency (2004).

[19] H. Vonach, M. Uhl, B. Strohmaier, B. W. Smith, E. G. Bilpuch, G. E. Mitchell, Phys. Rev. C **38**, 2541 (1988).

[20] R. B. Firestone, "Table of Isotopes," Eighth Edition, John Wiley & Sons, Inc. (1998).

[21] M. Baba, M. Ishikawa, N. Yabuta, T. Kikuchi, H. Wakabayashi, N. Hirakawa, *Proc. Int. Conf. Nuclear Data for Science and Technology,* Mito, Japan, 30 May – 3 Jun 1988, p. 291, Japan Atomic Energy Research Institute, Tokai-mura, (1988).

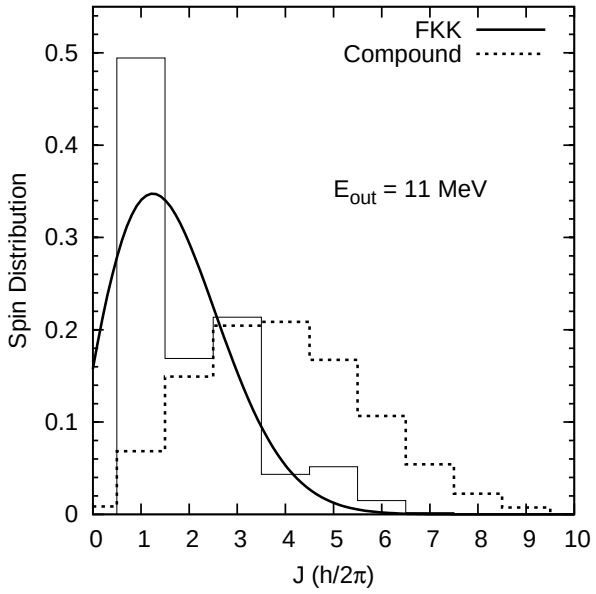


FIG. 1: Comparison of the spin distribution in the residual nucleus populated by the inelastic scattering, calculated with the FKK model (solid histogram), and with the compound nuclear model (dotted histogram). The neutron incident energy is 20 MeV and the out-going energy is 11 MeV. The smooth curve (solid line) is a Gaussian fit to the one-step FKK result.

[22] S. A. Wender, S. Balestrini, A. Brown, R. C. Haight, C. M. Laymon, T. M. Lee, P. W. Lisowski, W. McCorkle, R. O. Nelson, W. Parker, and H. W. Hill, Nucl. Instrum. Methods Phys. Res. A **336**, 226 (1993).

[23] R. O. Nelson, N. Fotiades, M. Devlin, J. A. Becker, P. E. Garrett, and W. Younes, *Proc. Int. Conf. Nuclear Data for Science and Technology,* Santa Fe, USA, 26 Sep – 1 Oct, p. 838, AIP Conference Proceedings, Melville, New York, (2005).

[24] D. P. McNabb, UCRL-ID-139906, Lawrence Livermore National Laboratory, (1999).

[25] W. Dilg, W. Schantl, H. Vonach, M. Uhl, Nucl. Phys., **A217** 269 (1973).

[26] S. I. Al-Quraishi, S. M. Grimes, T. N. Massey, D. A. Resler, Phys. Rev. C **67**, 015803 (2003).

[27] M. Al-Abyad, S. Sudár, M. N. H. Comsan, S. M. Qaim, Phys. Rev. C **73**, 064608 (2006).

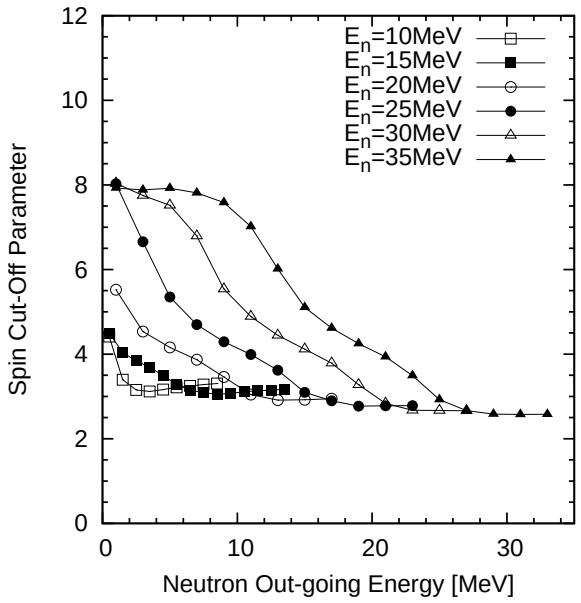


FIG. 2: Spin cut-off parameters for the FKK spin distribution for various neutron incident energies, as a function of excitation energy.

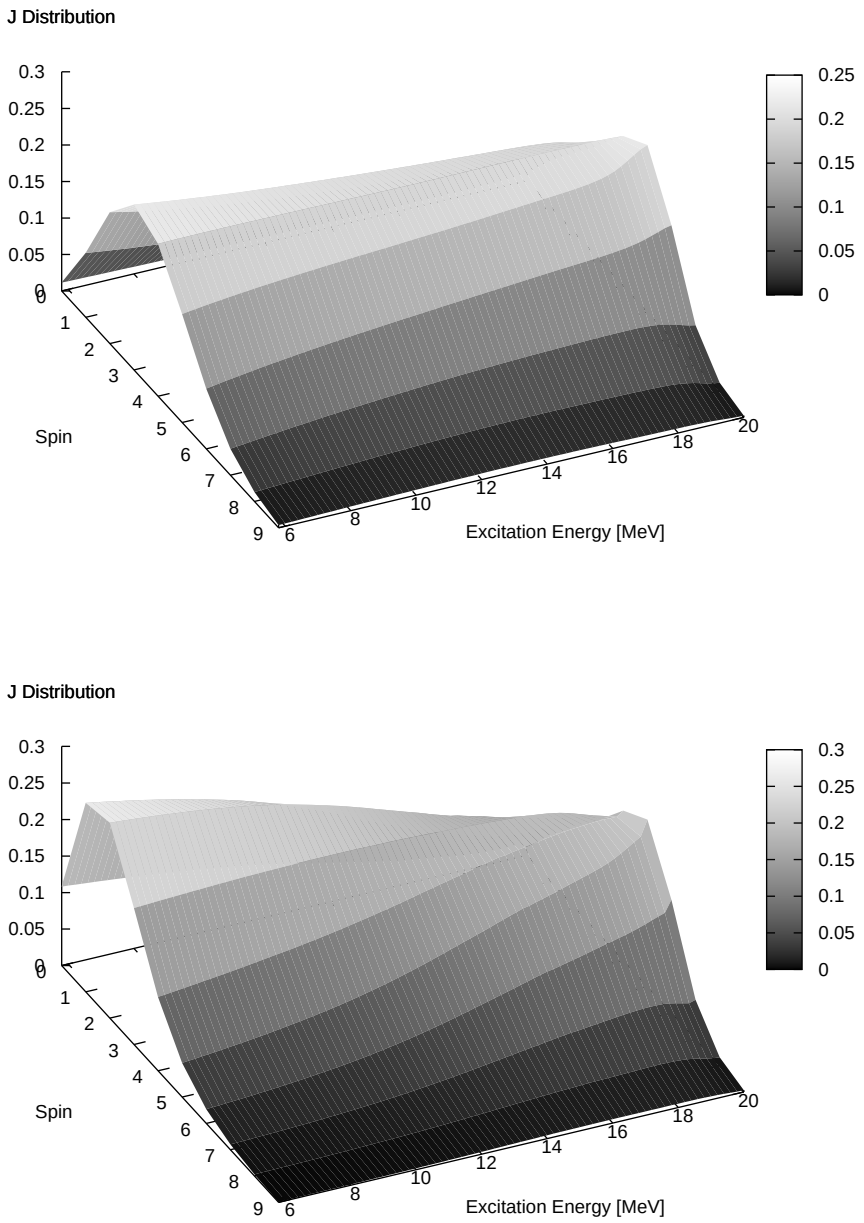


FIG. 3: The summed spin distributions in excited $^{48}$Ti following 20-MeV neutron inelastic scattering under different assumptions for the pre-equilibrium spin transfer. The upper panel shows the case when the pre-equilibrium spin distribution is assumed to be the same as for the compound reaction, as often assumed in the past. The bottom panel is the case when the FKK spin distribution is newly included in the GNASH calculations.

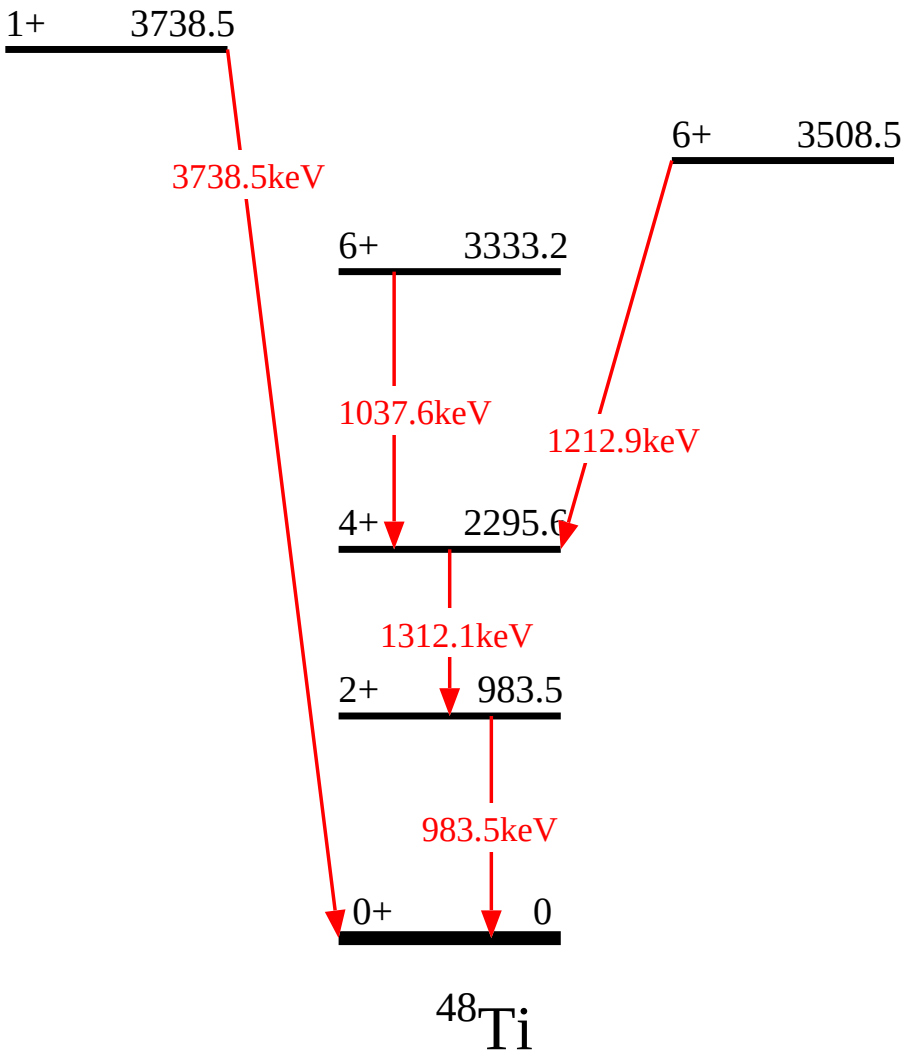


FIG. 4: Partial level scheme of $^{48}$Ti displaying transitions analyzed in the present work.

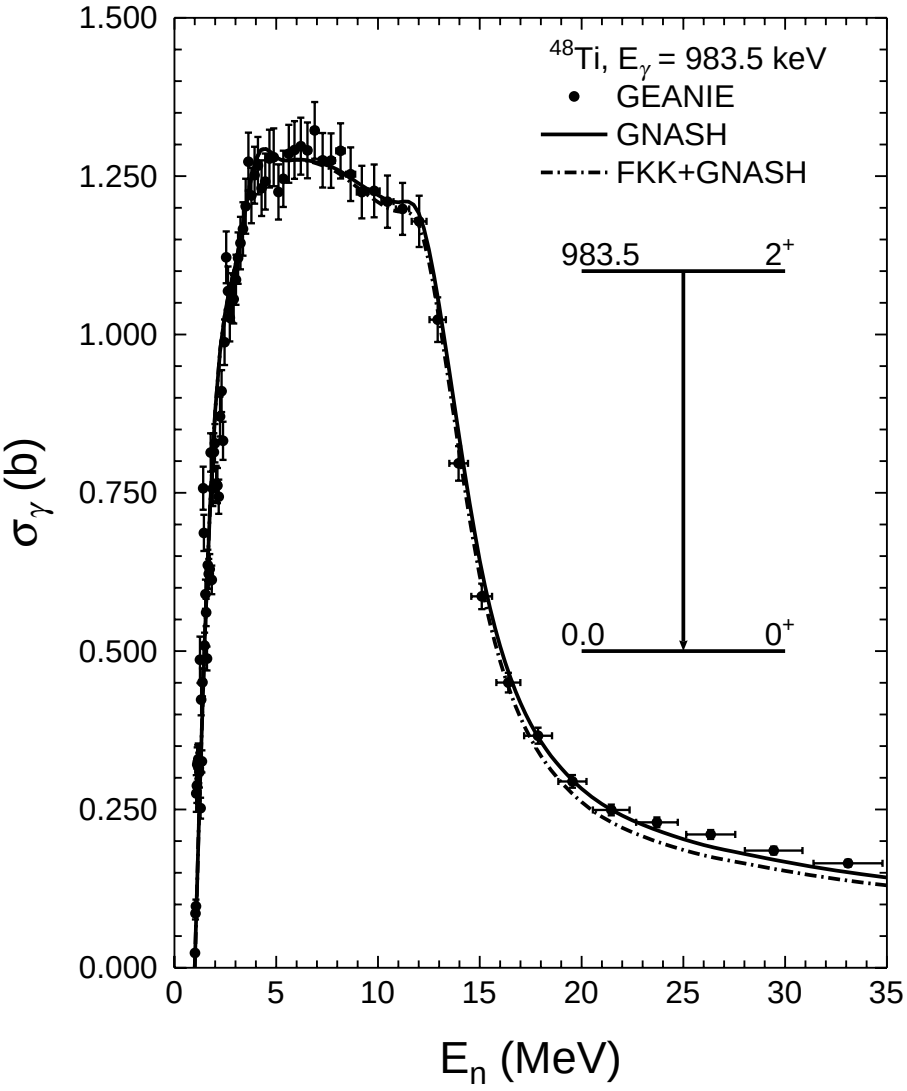


FIG. 5: Comparison of the 983-keV $\gamma$-ray production cross section with the experimental data [3]. The dashed line is the result of the FKK+GNASH calculation, and the solid line represents the result when the pre-equilibrium spin distribution is assumed to be the same as for the compound reaction.

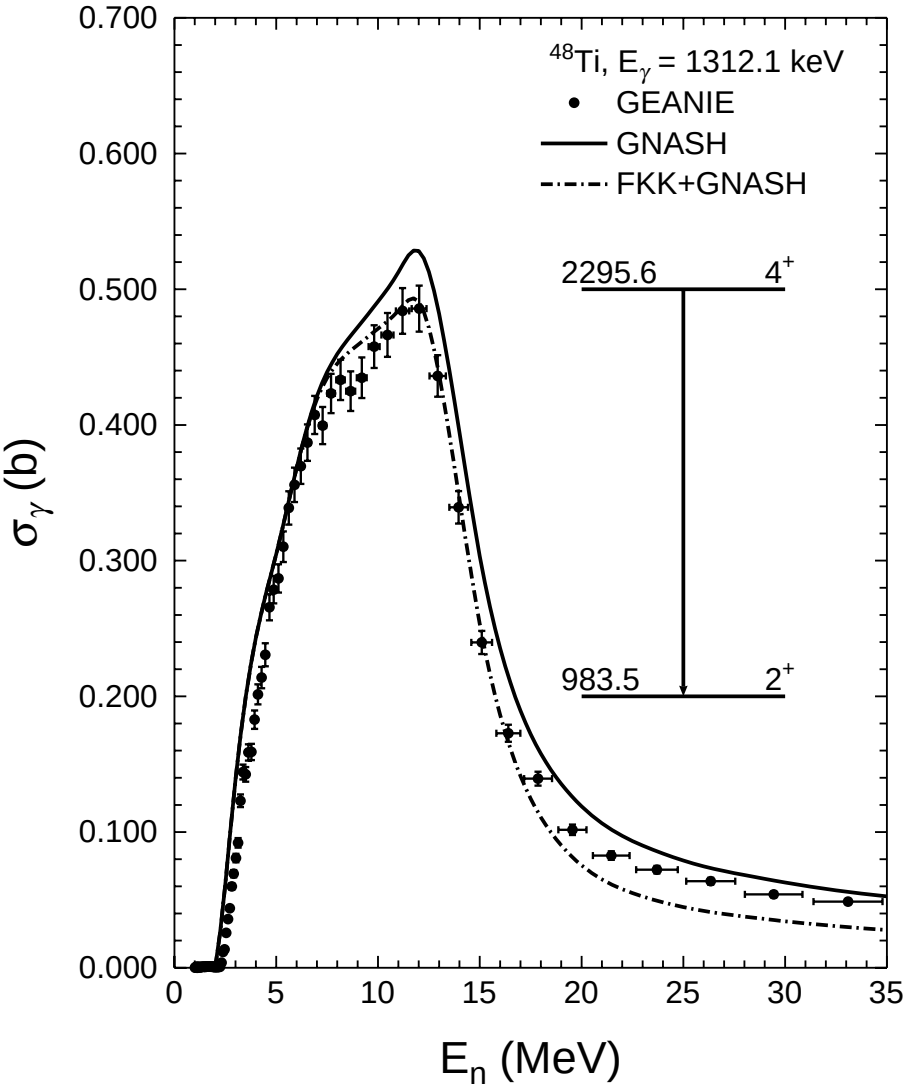


FIG. 6: Comparison of the 1312-keV $\gamma$-ray production cross section with the experimental data [3]. The dashed line is the result of the FKK+GNASH calculation, and the solid line represents the result when the pre-equilibrium spin distribution is assumed to be the same as for the compound reaction.

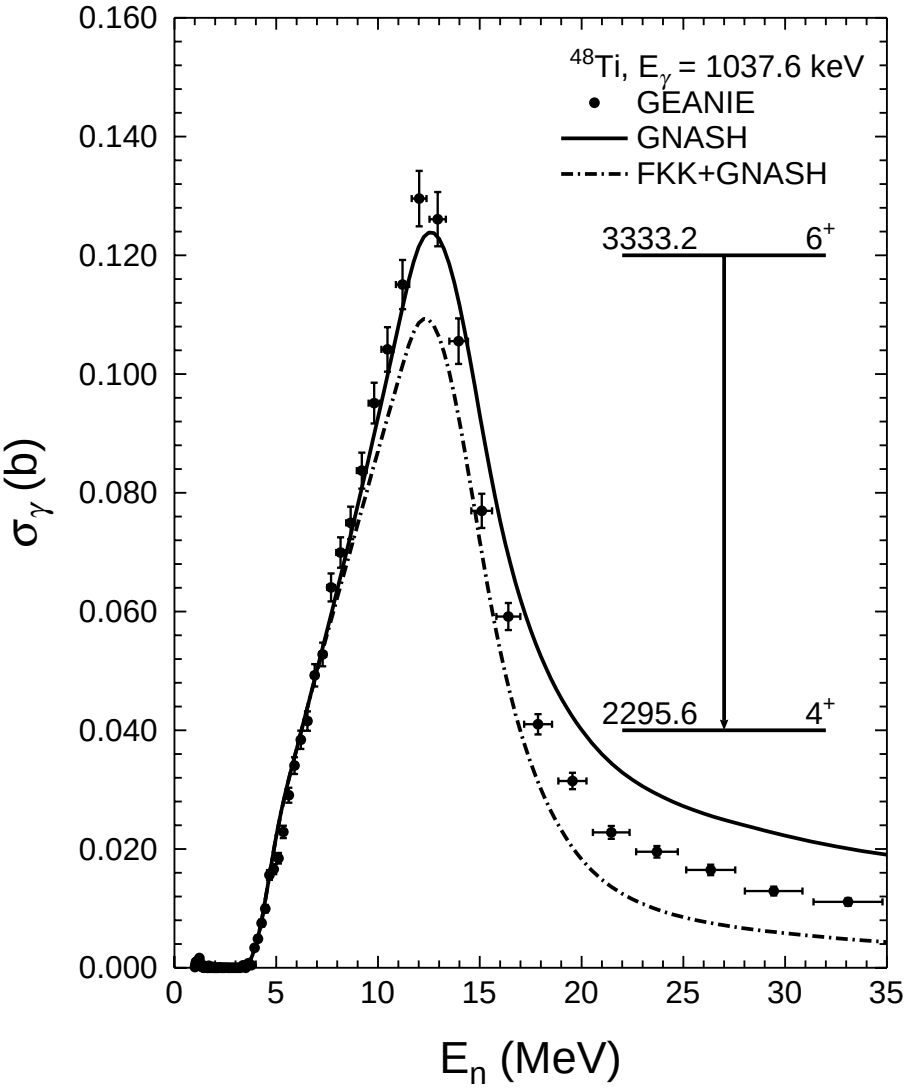


FIG. 7: Comparison of the 1037-keV $\gamma$-ray production cross section with the experimental data [3]. The dashed line is the result of the FKK+GNASH calculation, and the solid line represents the result when the pre-equilibrium spin distribution is assumed to be the same as for the compound reaction.

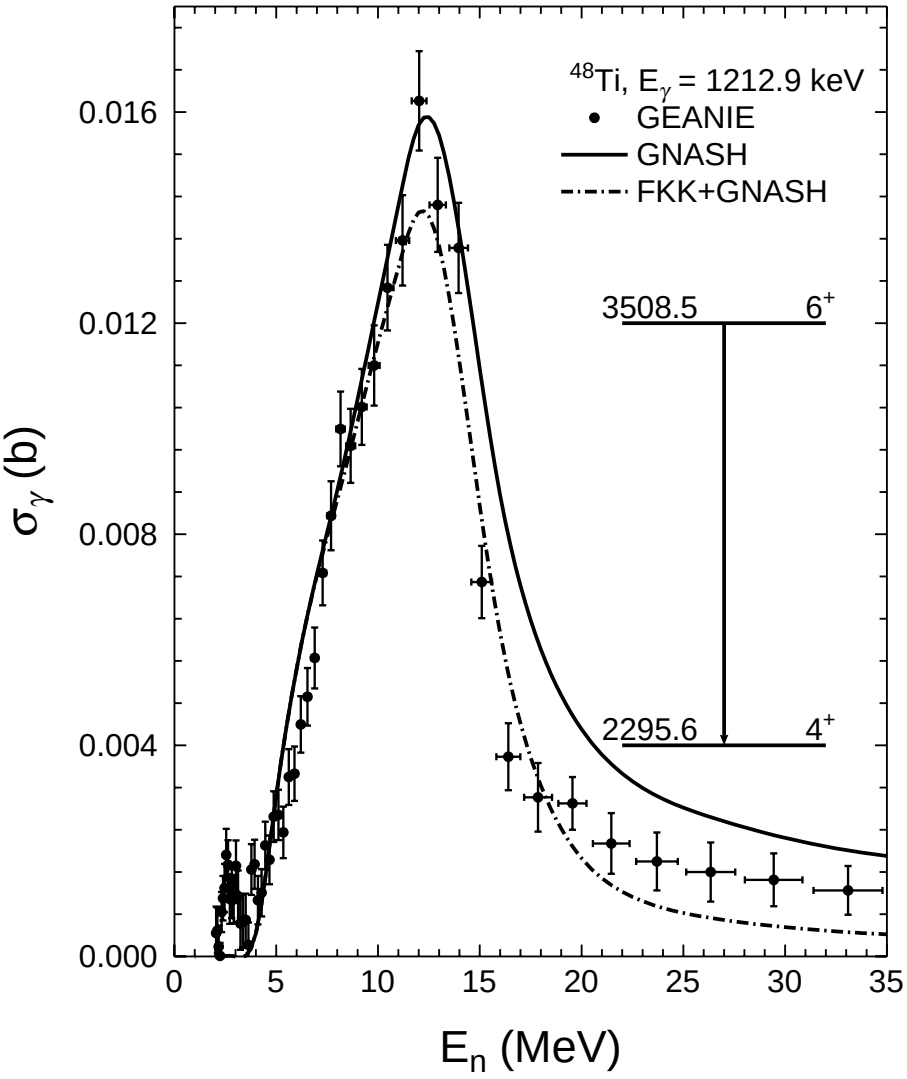


FIG. 8: Comparison of the 1213-keV $\gamma$-ray production cross section with the experimental data [3]. The dashed line is the result of the FKK+GNASH calculation, and the solid line represents the result when the pre-equilibrium spin distribution is assumed to be the same as for the compound reaction.

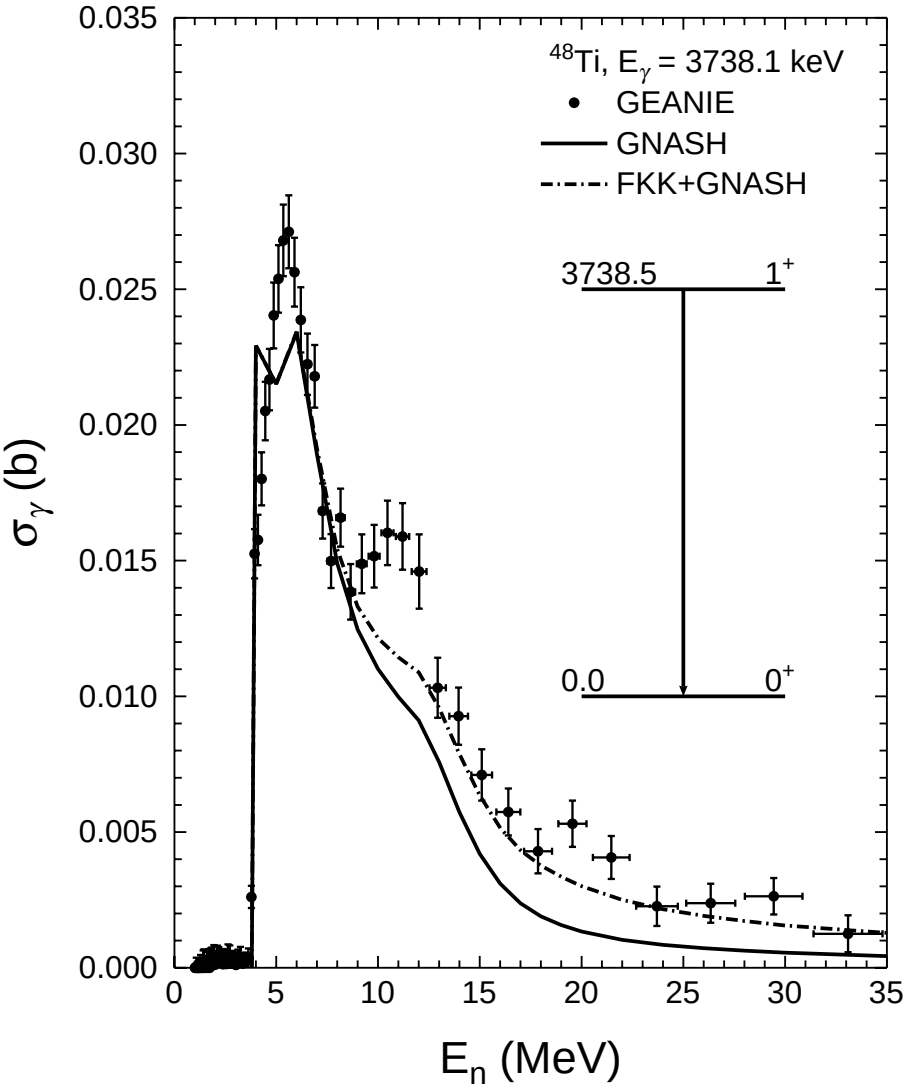


FIG. 9: Comparison of the 3737-keV $\gamma$-ray production cross section with the experimental data [3]. The dashed line is the result of the FKK+GNASH calculation, and the solid line represents the result when the pre-equilibrium spin distribution is assumed to be the same as for the compound reaction.

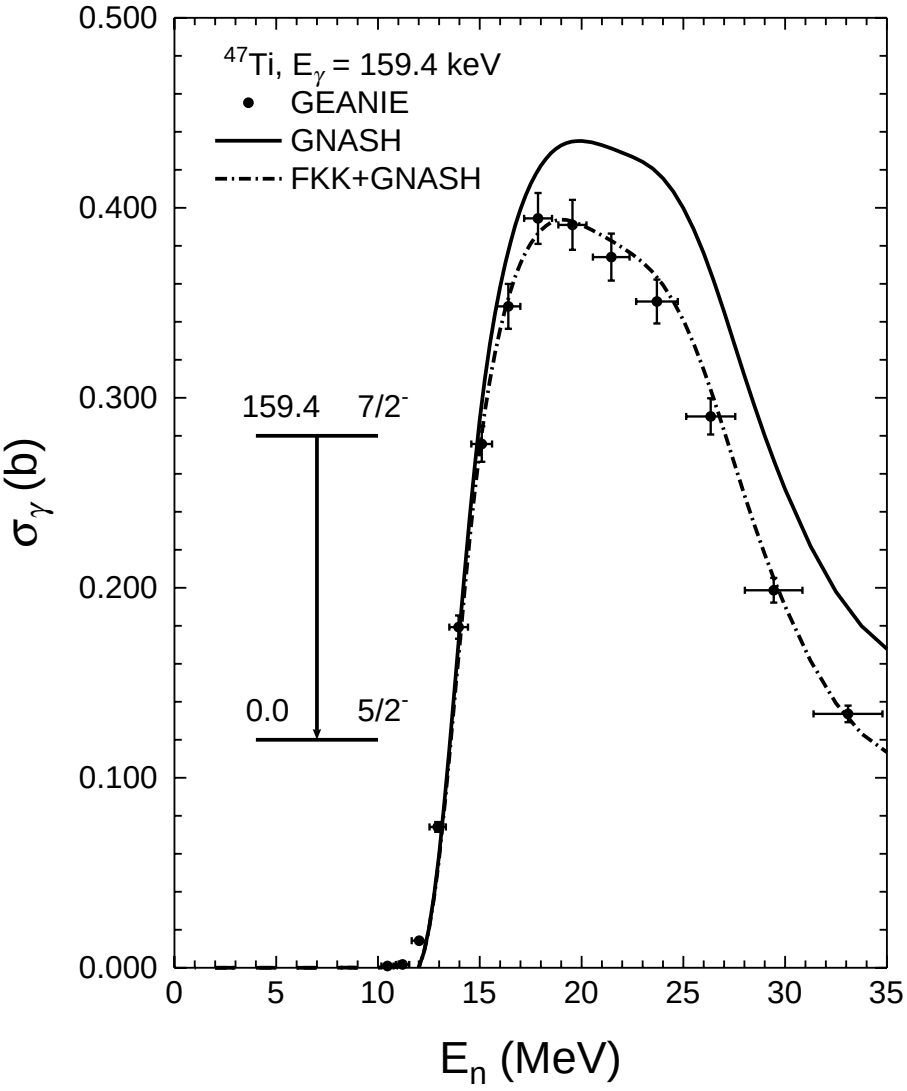


FIG. 10: Comparison of the 159-keV $\gamma$-ray production cross section in $^{47}$Ti with the experimental data [3]. The dashed line is the result of the FKK+GNASH calculation, and the solid line represents the result when the pre-equilibrium spin distribution is assumed to be the same as for the compound reaction.

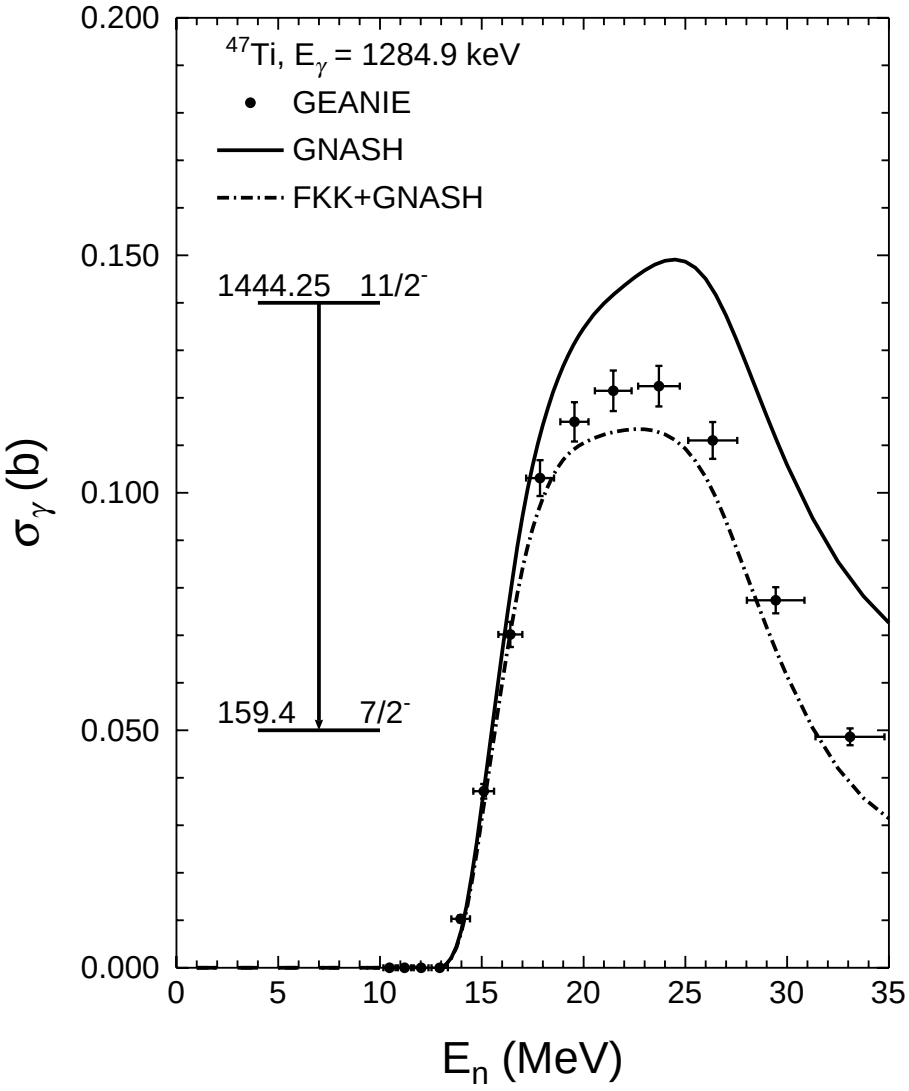


FIG. 11: Comparison of the 1285-keV $\gamma$-ray production cross section in $^{47}$Ti with the experimental data [3]. The dashed line is the result of the FKK+GNASH calculation, and the solid line represents the result when the pre-equilibrium spin distribution is assumed to be the same as for the compound reaction.

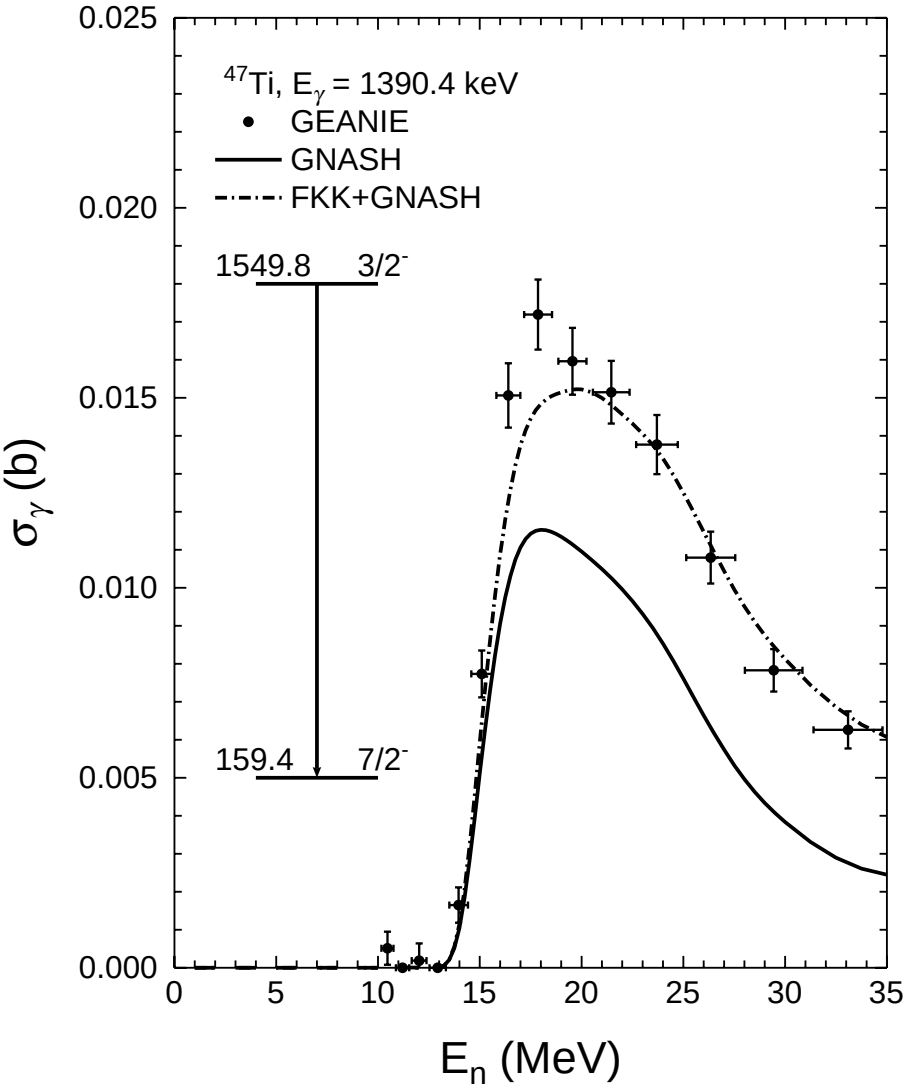


FIG. 12: Comparison of the 1390-keV $\gamma$-ray production cross section in $^{47}$Ti with the experimental data [3]. The dashed line is the result of the FKK+GNASH calculation, and the solid line represents the result when the pre-equilibrium spin distribution is assumed to be the same as for the compound reaction.

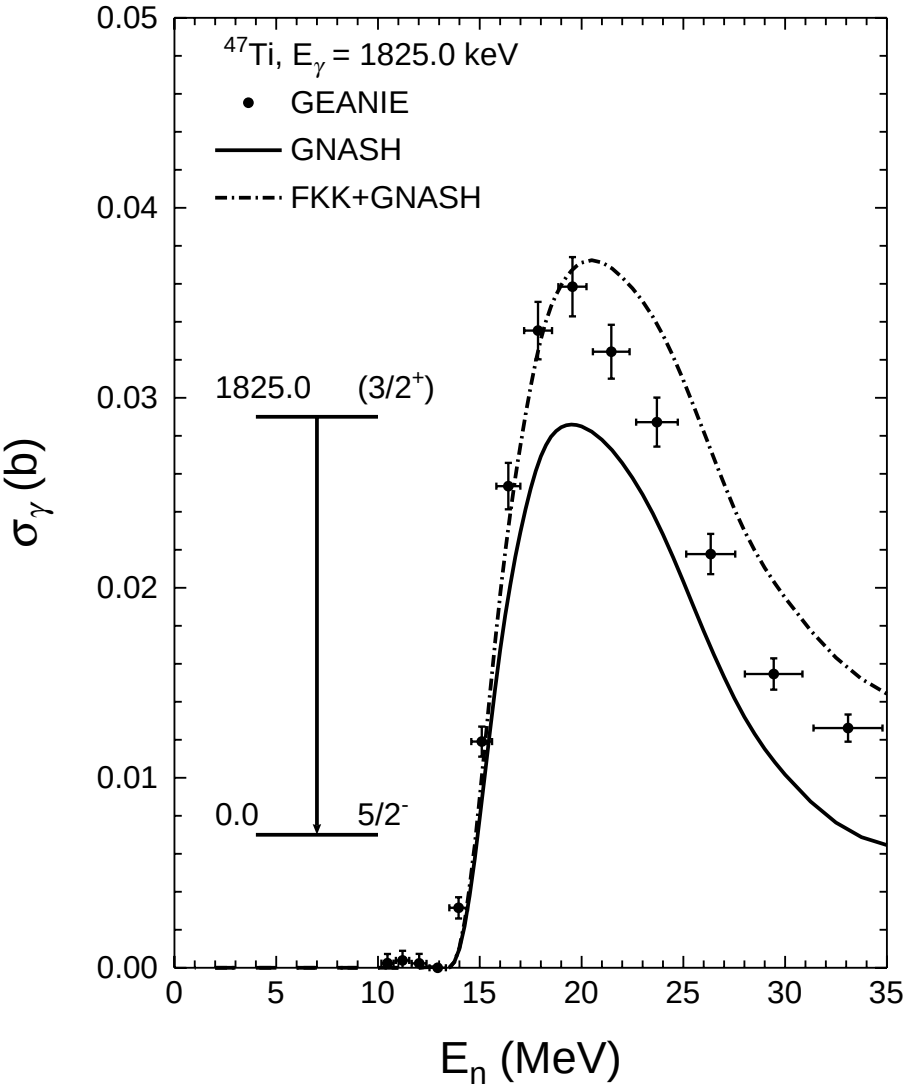


FIG. 13: Comparison of the 1825-keV $\gamma$-ray production cross section in $^{47}$Ti with the experimental data [3]. The dashed line is the result of the FKK+GNASH calculation, and the solid line represents the result when the pre-equilibrium spin distribution is assumed to be the same as for the compound reaction.